International Journal of Thermal Sciences 48 (2009) 1530–1541

Contents lists available at ScienceDirect

International Journal of Thermal Sciences

www.elsevier.com/locate/ijts

A stable finite difference scheme for thermal analysis in an *N*-carrier system

Weizhong Dai [a,*], Fei Zhu [a], Da Yu Tzou [b]

[a] Mathematics and Statistics, College of Engineering and Science, Louisiana Tech University, Ruston, LA 71272, USA
[b] Department of Mechanical and Aerospace Engineering, University of Missouri, Columbia, MO 65211, USA

ARTICLE INFO

Article history:
Received 27 May 2008
Received in revised form 10 November 2008
Accepted 14 January 2009
Available online 5 February 2009

Keywords:
Modeling for thermal analysis
N-carrier system
Energy exchange
Energy estimate
Finite difference scheme
Stability

ABSTRACT

In this study, we extend the concept of the well-known parabolic two-step model for micro heat transfer to model the energy exchanges in a generalized *N*-carrier system with heat sources. We show that the multi-carrier system satisfies an energy estimate. Based on this result, a finite difference scheme is then developed for thermal analysis in the multi-carrier system. The developed numerical scheme is shown to satisfy a discrete analogue of the energy estimate, implying that it is unconditionally stable. The method is illustrated by several numerical examples.

1. Introduction

Energy exchange between electrons and phonons in metal provides the best example in describing non-equilibrium heating during the ultrafast transient [1–6]. In times comparable to the thermalization and relaxation times of electrons and phonons, which are in the range from a few to several tens of picoseconds, heat continuously flows from hot electrons to cold phonons through mutual collisions. Consequently, electron temperature continuously decreases whereas phonon temperature continuously increases until thermal equilibrium is reached. Intensity of heat flow during non-equilibrium heating is proportional to the temperature difference between electrons and phonons. The proportional constant is termed the electron–phonon coupling factor, which is a new thermophysical property in microscale heat transfer [3,4,6,7]. The mathematical equations for describing the non-equilibrium heating can be expressed as a well-known parabolic two-step model [3,4]:

$$C_e \frac{\partial T_e(\vec{x},t)}{\partial t} = k_e \nabla^2 T_e(\vec{x},t) - G\big[T_e(\vec{x},t) - T_l(\vec{x},t)\big], \tag{1}$$

$$C_l \frac{\partial T_l(\vec{x},t)}{\partial t} = G\big[T_e(\vec{x},t) - T_l(\vec{x},t)\big], \tag{2}$$

where T_e and T_l are electron temperature and lattice temperature, respectively; C_e and C_l are heat capacities, k_e is the conductivity, G is the electron–phonon coupling factor, and ∇^2 is the Laplace operator.

The same concept has been extended to model pulsed heating on amorphous media [6] and non-equilibrium heat transport in porous media [8]. In place of electrons and phonons, energy coupling between the solid and fluid/gaseous phases was described in the same way. The thermalization and relaxation times for slow materials, such as lightly packed copper spheres or rough carbon surfaces [6,9], can reach several tenths of a millisecond due to the low-conducting phases involved in the assemblies. Transient times on the order of 10^{-4} s, therefore, are considered to be ultrafast because of the pronounced thermalization and relaxation behaviors observed in the sub-millisecond domain. Non-equilibrium heating porous media [8] already involve a more complicated system than the two-carrier (electron–phonon) system in metals. Phase change in wicked heat pipes, moreover, often involves non-equilibrium heating/energy dissipation among the solid wick, liquid, and vapor phases [10]. As extension is made to medical applications employing femtosecond lasers [11], complexities of non-equilibrium heating further evolve due to involvement of multiple carriers in biomedical systems, including hard/soft tissues (proteins), water, and minerals. The ways in which thermal energy is distributed among different carriers, as well as the characteristic times dictating the intrinsic behaviors of non-equilibrium heating, play a dominant role in assuring the success of femtosecond-laser technologies.

Recently, a new three-carrier system without heat sources, that generalizes the well-known parabolic two-step model in micro heat transfer, has been presented in the ASME Conference on Micro/Nano Heat Transfer (MNHT08), where the possible thermal lagging behavior in the new system was discussed [12]. In this article,

* Corresponding author. Tel.: +1 318 257 3301; fax: +1 318 257 2562.
E-mail address: dai@coes.latech.edu (W. Dai).

1290-0729/$ – see front matter
doi:10.1016/j.ijthermalsci.2009.01.007

Nomenclature

C_1, C_j, C_N	heat capacity	J/(m^3 K)
$G_{i,j}$	carrier i–carrier j coupling factor	W/(m^3 K)
k_i	thermal conductivity	W/(m K)
M	number of grid points	
L	length of interval	m
N	number of carriers	
Q_j	heat source	J/(m^3 s)
T_e, T_j, T_l	electron temperature, temperature of carrier j, lattice temperature	K
$(T_j)_m^n$	numerical solution of T_j at $(m\Delta x, n\Delta t)$	
t, t_0	time	s
$x, \vec{x}$	Cartesian coordinates	

Greek symbols

∇	gradient operator
$\nabla_x, \nabla_{\bar{x}}$	forward and backward finite difference operators, respectively
Δt	time increment
Δx	spatial grid size
$\vec{\eta}$	unit outward normal vector on the boundary $\partial\Omega$
Ω	interval or region

Subscripts

e	electron
i	the ith carrier
j	the jth carrier
l	lattice
m	the mth grid point

we extend this concept to model the energy exchanges in a generalized N-carrier system with heat sources as follows:

$$C_1\frac{\partial T_1(\vec{x},t)}{\partial t} = \nabla\cdot\big(k_1\nabla T_1(\vec{x},t)\big) - \sum_{i=2}^{N} G_{1,i}\big[T_1(\vec{x},t) - T_i(\vec{x},t)\big] + Q_1(\vec{x},t), \tag{3}$$

$$C_j\frac{\partial T_j(\vec{x},t)}{\partial t} = \nabla\cdot\big(k_j\nabla T_j(\vec{x},t)\big) + \sum_{i=1}^{j-1} G_{i,j}\big[T_i(\vec{x},t) - T_j(\vec{x},t)\big] - \sum_{i=j+1}^{N} G_{j,i}\big[T_j(\vec{x},t) - T_i(\vec{x},t)\big] + Q_j(\vec{x},t), \tag{4}$$

$j = 2,\ldots,N-1,$

$$C_N\frac{\partial T_N(\vec{x},t)}{\partial t} = \nabla\cdot\big(k_N\nabla T_N(\vec{x},t)\big) + \sum_{i=1}^{N-1} G_{i,N}\big[T_i(\vec{x},t) - T_N(\vec{x},t)\big] + Q_N(\vec{x},t), \tag{5}$$

where T_i $(i=1,\ldots,N)$ are temperatures, C_i $(i=1,\ldots,N)$ are heat capacities and constants, k_i $(i=1,\ldots,N)$ are conductivities, $G_{i,j}$ is the carrier i–carrier j coupling factor and is assumed to be positive constant, and Q_i $(i=1,\ldots,N)$ are heat sources. Here, $(\vec{x},t)$ is in $\Omega\times[0,t_0]$, where Ω is assumed to be an interval in the 1D case or a rectangular region in the 2D or 3D case. The summations with negative/positive signs in the front represent the energy lost/gained to/from other carriers. The first summation in the second expression, for example, represents the volumetric energy density received by carrier j, whereas the second summation in the same equation represents the energy density released from carrier j. Non-equilibrium heating is reflected by the temperature differences in the system. After thermalization where thermal equilibrium is achieved among N carriers, all G-terms in the system diminish and Fourier diffusion is recovered. Here, we assume that (1) different energy carriers are in perfect thermal contact, (2) the coupling factors $G_{i,j}$ only depend on the physical properties of the carriers and not on the presence (or absence) of impurities among these carriers, (3) thermal radiation exchange between these energy carriers is ignored, and (4) all N carriers are stationary in the system. Fig. 1 shows the energy exchanges among dissimilar energy carriers, which are assumed proportional to their temperature differences as that assumed during electron–phonon coupling [1–5].

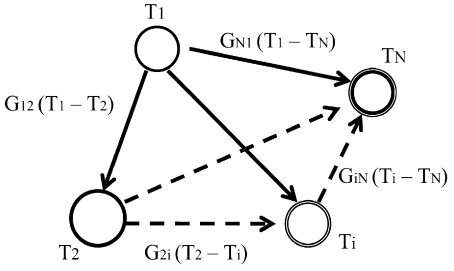

Fig. 1. Energy exchanges in a system with N carriers.

Although the values of coupling factors $G_{i,j}$ in multi-carrier systems have not yet been determined in realistic engineering applications and the ongoing research is still at an early stage, it is of interest to develop a numerical method for solving the above N-carrier system because the system could be complicated when N is large. In this study, we will develop a stable finite difference scheme for thermal analysis in the generalized N-carrier system. To this end, we first analyze the energy conservation in the N-carrier system and show that the system satisfies an energy estimate. The numerical scheme is then obtained by satisfying a discrete analogue of the energy estimate. Finally, the method is illustrated by several numerical examples.

2. Energy estimate

We assume that there are no heat losses from the system in the short time response [6]. As such, the boundary condition for T_i $(i=1,\ldots,N)$ is

$$\frac{\partial T_i(\vec{x},t)}{\partial\vec{\eta}} = 0, \quad i=1,\ldots,N;\ (\vec{x},t)\in\partial\Omega\times[0,t_0], \tag{6}$$

where $\vec{\eta}$ is the unit outward normal vector on the boundary $\partial\Omega$. To obtain an energy estimate, we multiply Eqs. (3)–(5) by $T_1(\vec{x},t)$, $T_j(\vec{x},t)$, and $T_N(\vec{x},t)$, respectively, integrate them over Ω, and add the results together. This gives

$$\int_\Omega \sum_{i=1}^{N} C_i T_i\frac{\partial T_i}{\partial t}\,d\Omega = \int_\Omega \sum_{i=1}^{N} T_i\nabla\cdot(k_i\nabla T_i)\,d\Omega - \int_\Omega \sum_{\substack{i,j=1\\ i<j}}^{N} G_{i,j}[T_i - T_j]^2\,d\Omega + \int_\Omega \sum_{i=1}^{N} T_i Q_i\,d\Omega. \tag{7}$$

The left-hand side (LHS) of the above equation can be written as

$$\int_{\Omega}\sum_{i=1}^{N} C_i T_i \frac{\partial T_i}{\partial t}\,d\Omega = \frac{d}{dt}\int_{\Omega}\frac{1}{2}\sum_{i=1}^{N} C_i T_i^2\,d\Omega. \tag{8}$$

Using the integration-by-parts formula (*i.e.*, $\int_{\Omega} u_x v\,d\Omega = -\int_{\Omega} u v_x\,d\Omega + \int_{\partial\Omega} u v \eta_x\,d\partial\Omega$, where η_x is a component of $\vec{\eta}$ [13], with $u = k_i\frac{\partial T_i}{\partial x}$ and $v = T_i$) and the boundary condition ($\frac{\partial T_i}{\partial \eta} = 0$ on the boundary), one may obtain

$$\begin{aligned}
&\int_{\Omega}\sum_{i=1}^{N} T_i \nabla\cdot(k_i\nabla T_i)\,d\Omega \\
&\quad = -\int_{\Omega}\sum_{i=1}^{N} k_i(\nabla T_i)^2\,d\Omega + \sum_{i=1}^{N}\int_{\partial\Omega} k_i T_i\frac{\partial T_i}{\partial\vec{\eta}}\,d\partial\Omega \\
&\quad = -\int_{\Omega}\sum_{i=1}^{N} k_i(\nabla T_i)^2\,d\Omega.
\end{aligned} \tag{9}$$

By Cauchy–Schwarz's inequality (*i.e.*, $2ab \leqslant \varepsilon a^2 + \frac{1}{\varepsilon}b^2$, where $\varepsilon > 0$ [13]), we obtain

$$\int_{\Omega}\sum_{i=1}^{N} T_i Q_i\,d\Omega \leqslant \int_{\Omega}\frac{1}{2}\sum_{i=1}^{N} C_i T_i^2\,d\Omega + \frac{1}{2}\int_{\Omega}\sum_{i=1}^{N}\frac{1}{C_i}Q_i^2\,d\Omega. \tag{10}$$

Substituting Eqs. (8)–(10) into Eq. (7) gives

$$\begin{aligned}
&\frac{d}{dt}\int_{\Omega}\frac{1}{2}\sum_{i=1}^{N} C_i T_i^2\,d\Omega + \int_{\Omega}\sum_{i=1}^{N} k_i(\nabla T_i)^2\,d\Omega \\
&\qquad + \int_{\Omega}\sum_{\substack{i,j=1\\ i<j}}^{N} G_{i,j}[T_i - T_j]^2\,d\Omega \\
&\quad \leqslant \int_{\Omega}\frac{1}{2}\sum_{i=1}^{N} C_i T_i^2\,d\Omega + \frac{1}{2}\int_{\Omega}\sum_{i=1}^{N}\frac{1}{C_i}Q_i^2\,d\Omega.
\end{aligned} \tag{11}$$

Taking out the second and third terms on the LHS because they are non-negative, introducing $F(t) = \int_{\Omega}\sum_{i=1}^{N} C_i T_i^2\,d\Omega$ and $Q(t) = \int_{\Omega}\sum_{i=1}^{N}\frac{1}{C_i}Q_i^2\,d\Omega$, and then integrating it with respect to t, Eq. (11) can be further simplified as follows:

$$F(t) - F(0) \leqslant \int_0^t F(s)\,ds + \int_0^t Q(s)\,ds. \tag{12}$$

By Gronwall's lemma (*i.e.*, if $\phi(t) \geqslant 0$ and $\psi(t) \geqslant 0$ are continuous functions such that $\phi(t) \leqslant K + L\int_{t_0}^{t}\psi(s)\phi(s)\,ds$ holds on $t_0 \leqslant t \leqslant t_1$, where K and L are positive constants, then $\phi(t) \leqslant K\exp(L\int_{t_0}^{t}\psi(s)\,ds)$ on $t_0 \leqslant t \leqslant t_1$, see [13]), we obtain for $0 \leqslant t \leqslant t_0$,

$$\begin{aligned}
F(t) &\leqslant \int_0^t 1\cdot F(s)\,ds + \left[F(0) + \int_0^t Q(s)\,ds\right] \\
&\leqslant e^t\left[F(0) + \int_0^t Q(s)\,ds\right],
\end{aligned} \tag{13}$$

and hence the following energy estimate for the N-carrier system has been obtained

$$\begin{aligned}
&\int_{\Omega}\sum_{i=1}^{N} C_i T_i^2(\vec{x},t)\,d\Omega \\
&\quad \leqslant e^t\left[\int_{\Omega}\sum_{i=1}^{N} C_i T_i^2(\vec{x},0)\,d\Omega + \int_0^t\int_{\Omega}\sum_{i=1}^{N}\frac{1}{C_i}Q_i^2(\vec{x},s)\,d\Omega\,ds\right],
\end{aligned} \tag{14}$$

for $0 \leqslant t \leqslant t_0$ and t_0 is a constant.

It should be pointed out that the energy estimation is helpful for developing a numerical scheme. It is desirable that the developed numerical scheme should have a discrete analogue of the energy estimation, which may be helpful for analyzing the stability of finite difference schemes [14–16].

3. Finite difference scheme

To develop a finite difference scheme, which satisfies a discrete analogue of Eq. (14), we consider the system in one dimension for simplicity. We denote $(T_i)_m^n$ as the numerical approximation of $(T_i)(m\triangle x, n\triangle t)$, where Δx and $\triangle t$ are the x-directional spatial and temporal mesh sizes, respectively, and $0 \leqslant m \leqslant M$ so that $M\triangle x = L$, where L is the length of the interval $[0, L]$. Furthermore, the first-order forward and backward finite difference operators are defined as

$$\nabla_x u_m = \frac{u_{m+1} - u_m}{\triangle x}, \qquad \nabla_{\bar{x}} u_m = \frac{u_m - u_{m-1}}{\triangle x}.$$

Thus, a Crank–Nicholson type finite difference scheme for solving Eqs. (3)–(5) in one dimension can be developed as

$$\begin{aligned}
&C_1\frac{(T_1)_m^{n+1} - (T_1)_m^n}{\triangle t} \\
&\quad = \nabla_x\cdot\left[(k_1)_{m-\frac{1}{2}}^{n+\frac{1}{2}}\nabla_{\bar{x}}\left(\frac{(T_1)_m^{n+1} + (T_1)_m^n}{2}\right)\right] \\
&\qquad - \sum_{i=2}^{N} G_{1,i}\left[\frac{(T_1)_m^{n+1} + (T_1)_m^n}{2} - \frac{(T_i)_m^{n+1} + (T_i)_m^n}{2}\right] + (Q_1)_m^{n+\frac{1}{2}},
\end{aligned} \tag{15}$$

$$\begin{aligned}
&C_j\frac{(T_j)_m^{n+1} - (T_j)_m^n}{\triangle t} \\
&\quad = \nabla_x\cdot\left[(k_j)_{m-\frac{1}{2}}^{n+\frac{1}{2}}\nabla_{\bar{x}}\left(\frac{(T_j)_m^{n+1} + (T_j)_m^n}{2}\right)\right] \\
&\qquad + \sum_{i=1}^{j-1} G_{i,j}\left[\frac{(T_i)_m^{n+1} + (T_i)_m^n}{2} - \frac{(T_j)_m^{n+1} + (T_j)_m^n}{2}\right] \\
&\qquad - \sum_{i=j+1}^{N} G_{j,i}\left[\frac{(T_j)_m^{n+1} + (T_j)_m^n}{2} - \frac{(T_i)_m^{n+1} + (T_i)_m^n}{2}\right] + (Q_j)_m^{n+\frac{1}{2}}, \\
&\quad j = 2,\ldots,N-1,
\end{aligned} \tag{16}$$

$$\begin{aligned}
&C_N\frac{(T_N)_m^{n+1} - (T_N)_m^n}{\triangle t} \\
&\quad = \nabla_x\cdot\left[(k_N)_{m-\frac{1}{2}}^{n+\frac{1}{2}}\nabla_{\bar{x}}\left(\frac{(T_N)_m^{n+1} + (T_N)_m^n}{2}\right)\right] \\
&\qquad + \sum_{i=1}^{N-1} G_{i,N}\left[\frac{(T_i)_m^{n+1} + (T_i)_m^n}{2} - \frac{(T_N)_m^{n+1} + (T_N)_m^n}{2}\right] + (Q_N)_m^{n+\frac{1}{2}},
\end{aligned} \tag{17}$$

where $m = 1, 2, \ldots, M-1$. It can be seen that the truncation error of the above scheme at grid point $(m\Delta x, n\Delta t)$ is $O(\Delta t^2 + \Delta x^2)$. The boundary condition is discretized as follows:

$$(T_i)_0^n = (T_i)_1^n, \qquad (T_i)_M^n = (T_i)_{M-1}^n, \quad i = 1,\ldots,N, \tag{18}$$

for any time level n.

To obtain a discrete energy estimate which is an analogue of Eq. (14), we multiply Eq. (15) by $\Delta x\frac{(T_1)_m^{n+1}+(T_1)_m^n}{2}$, Eq. (16) by $\Delta x\frac{(T_j)_m^{n+1}+(T_j)_m^n}{2}$, and Eq. (17) by $\Delta x\frac{(T_N)_m^{n+1}+(T_N)_m^n}{2}$, sum m over $1\leqslant m\leqslant M-1$, and then add the results together. This gives

$$\begin{aligned}
&\frac{\Delta x}{\Delta t}\sum_{i=1}^{N}\frac{C_i}{2}\sum_{m=1}^{M-1}\left\{\left[(T_i)_m^{n+1}\right]^2-\left[(T_i)_m^n\right]^2\right\}\\
&\quad=\Delta x\sum_{i=1}^{N}\sum_{m=1}^{M-1}\left\{\nabla_x\cdot\left[(k_i)_{m-\frac12}^{n+\frac12}\nabla_{\bar x}\left(\frac{(T_i)_m^{n+1}+(T_i)_m^n}{2}\right)\right]\right\}\\
&\qquad\times\left[\frac{(T_i)_m^{n+1}+(T_i)_m^n}{2}\right]\\
&\qquad-\Delta x\sum_{\substack{i=1\\i<j}}^{N}\sum_{m=1}^{M-1}G_{i,j}\left[\frac{(T_i)_m^{n+1}+(T_i)_m^n}{2}-\frac{(T_j)_m^{n+1}+(T_j)_m^n}{2}\right]^2\\
&\qquad+\Delta x\sum_{i=1}^{N}\sum_{m=1}^{M-1}(Q_i)_m^{n+\frac12}\frac{(T_i)_m^{n+1}+(T_i)_m^n}{2}.
\end{aligned}\tag{19}$$

Using the summation by parts and then using Eq. (18), we can simply the first term on the right-hand side of Eq. (19) as follows:

First term

$$\begin{aligned}
&=\sum_{i=1}^{N}\sum_{m=1}^{M-1}\left[(k_i)_{m+\frac12}^{n+\frac12}\nabla_{\bar x}\left(\frac{(T_i)_{m+1}^{n+1}+(T_i)_{m+1}^n}{2}\right)\right]\\
&\quad\times\left[\frac{(T_i)_m^{n+1}+(T_i)_m^n}{2}\right]\\
&\quad-\sum_{i=1}^{N}\sum_{m=1}^{M-1}\left[(k_i)_{m-\frac12}^{n+\frac12}\nabla_{\bar x}\left(\frac{(T_i)_m^{n+1}+(T_i)_m^n}{2}\right)\right]\\
&\quad\times\left[\frac{(T_i)_m^{n+1}+(T_i)_m^n}{2}\right]\\
&=\sum_{i=1}^{N}\sum_{m=2}^{M}\left[(k_i)_{m-\frac12}^{n+\frac12}\nabla_{\bar x}\left(\frac{(T_i)_m^{n+1}+(T_i)_m^n}{2}\right)\right]\\
&\quad\times\left[\frac{(T_i)_{m-1}^{n+1}+(T_i)_{m-1}^n}{2}\right]\\
&\quad-\sum_{i=1}^{N}\sum_{m=1}^{M-1}\left[(k_i)_{m-\frac12}^{n+\frac12}\nabla_{\bar x}\left(\frac{(T_i)_m^{n+1}+(T_i)_m^n}{2}\right)\right]\\
&\quad\times\left[\frac{(T_i)_m^{n+1}+(T_i)_m^n}{2}\right]\\
&=\sum_{i=1}^{N}\sum_{m=1}^{M-1}\left[(k_i)_{m-\frac12}^{n+\frac12}\nabla_{\bar x}\left(\frac{(T_i)_m^{n+1}+(T_i)_m^n}{2}\right)\right]\\
&\quad\times\left[\frac{(T_i)_{m-1}^{n+1}+(T_i)_{m-1}^n}{2}\right]\\
&\quad-\sum_{i=1}^{N}\sum_{m=1}^{M-1}\left[(k_i)_{m-\frac12}^{n+\frac12}\nabla_{\bar x}\left(\frac{(T_i)_m^{n+1}+(T_i)_m^n}{2}\right)\right]\\
&\quad\times\left[\frac{(T_i)_m^{n+1}+(T_i)_m^n}{2}\right]\\
&=-\Delta x\sum_{i=1}^{N}\sum_{m=1}^{M-1}(k_i)_{m-\frac12}^{n+\frac12}\left[\nabla_{\bar x}\left(\frac{(T_i)_m^{n+1}+(T_i)_m^n}{2}\right)\right]^2.
\end{aligned}\tag{20}$$

Here, we have used the fact that

$$\begin{aligned}
\nabla_{\bar x}\left(\frac{(T_i)_M^{n+1}+(T_i)_M^n}{2}\right)&=\frac{1}{2\Delta x}\left\{\left[(T_i)_M^{n+1}+(T_i)_M^n\right]\right.\\
&\quad\left.-\left[(T_i)_{M-1}^{n+1}+(T_i)_{M-1}^n\right]\right\}=0,
\end{aligned}$$

and

$$\begin{aligned}
\nabla_{\bar x}\left(\frac{(T_i)_1^{n+1}+(T_i)_1^n}{2}\right)&=\frac{1}{2\Delta x}\left\{\left[(T_i)_1^{n+1}+(T_i)_1^n\right]\right.\\
&\quad\left.-\left[(T_i)_0^{n+1}+(T_i)_0^n\right]\right\}=0
\end{aligned}$$

based on Eq. (18). Furthermore, by Cauchy–Schwarz's inequality, we have

$$\begin{aligned}
&\Delta x\sum_{i=1}^{N}\sum_{m=1}^{M-1}(Q_i)_m^{n+\frac12}\frac{(T_i)_m^{n+1}+(T_i)_m^n}{2}\\
&\quad=\frac12\Delta x\sum_{i=1}^{N}\sum_{m=1}^{M-1}(Q_i)_m^{n+\frac12}(T_i)_m^{n+1}+\frac12\Delta x\sum_{i=1}^{N}\sum_{m=1}^{M-1}(Q_i)_m^{n+\frac12}(T_i)_m^n\\
&\quad\leqslant\frac14\Delta x\sum_{i=1}^{N}\sum_{m=1}^{M-1}C_i\left[(T_i)_m^{n+1}\right]^2+\frac14\Delta x\sum_{i=1}^{N}\sum_{m=1}^{M-1}\frac{1}{C_i}\left[(Q_i)_m^{n+\frac12}\right]^2\\
&\qquad+\frac14\Delta x\sum_{i=1}^{N}\sum_{m=1}^{M-1}C_i\left[(T_i)_m^n\right]^2+\frac14\Delta x\sum_{i=1}^{N}\sum_{m=1}^{M-1}\frac{1}{C_i}\left[(Q_i)_m^{n+\frac12}\right]^2\\
&\quad=\frac14\Delta x\sum_{i=1}^{N}\sum_{m=1}^{M-1}C_i\left\{\left[(T_i)_m^{n+1}\right]^2+\left[(T_i)_m^n\right]^2\right\}\\
&\qquad+\frac{\Delta x}{2}\sum_{i=1}^{N}\sum_{m=1}^{M-1}\frac{1}{C_i}\left[(Q_i)_m^{n+\frac12}\right]^2.
\end{aligned}\tag{21}$$

Substituting Eqs. (20)–(21) into Eq. (19) gives

$$\begin{aligned}
&\frac{1}{\Delta t}\left\{\Delta x\sum_{i=1}^{N}C_i\sum_{m=1}^{M-1}\left[(T_i)_m^{n+1}\right]^2-\Delta x\sum_{i=1}^{N}C_i\sum_{m=1}^{M-1}\left[(T_i)_m^n\right]^2\right\}\\
&\qquad+2\Delta x\sum_{i=1}^{N}\sum_{m=1}^{M-1}(k_i)_{m-\frac12}^{n+\frac12}\left[\nabla_{\bar x}\left(\frac{(T_i)_m^{n+1}+(T_i)_m^n}{2}\right)\right]^2\\
&\qquad+2\Delta x\sum_{\substack{i=1\\i<j}}^{N}\sum_{m=1}^{M-1}G_{i,j}\left[\frac{(T_i)_m^{n+1}+(T_i)_m^n}{2}-\frac{(T_j)_m^{n+1}+(T_j)_m^n}{2}\right]^2\\
&\quad\leqslant\frac{\Delta x}{2}\sum_{i=1}^{N}\sum_{m=1}^{M-1}C_i\left\{\left[(T_i)_m^{n+1}\right]^2+\left[(T_i)_m^n\right]^2\right\}\\
&\qquad+\Delta x\sum_{i=1}^{N}\sum_{m=1}^{M-1}\frac{1}{C_i}\left[(Q_i)_m^{n+\frac12}\right]^2.
\end{aligned}\tag{22}$$

Taking out the second and third terms on the LHS of Eq. (22) since they are non-negative, one may simplify Eq. (22) as

$$\begin{aligned}
&\Delta x\sum_{i=1}^{N}C_i\sum_{m=1}^{M-1}\left[(T_i)_m^{n+1}\right]^2-\Delta x\sum_{i=1}^{N}C_i\sum_{m=1}^{M-1}\left[(T_i)_m^n\right]^2\\
&\quad\leqslant\frac{\Delta t}{2}\Delta x\sum_{i=1}^{N}\sum_{m=1}^{M-1}C_i\left\{\left[(T_i)_m^{n+1}\right]^2+\left[(T_i)_m^n\right]^2\right\}\\
&\qquad+\Delta t\Delta x\sum_{i=1}^{N}\sum_{m=1}^{M-1}\frac{1}{C_i}\left[(Q_i)_m^{n+\frac12}\right]^2.
\end{aligned}\tag{23}$$

If we denote

$$\tilde F(n)=\Delta x\sum_{i=1}^{N}C_i\sum_{m=1}^{M-1}\left[(T_i)_m^n\right]^2$$

and

$$\tilde{Q}(n+1)=\Delta x\sum_{i=1}^{N}\sum_{m=1}^{M-1}\frac{1}{C_i}\left[(Q_i)_m^{n+\frac{1}{2}}\right]^2,$$

then Eq. (23) can be further simplified as follows:

$$\left(1-\frac{\Delta t}{2}\right)\tilde{F}(n+1)\leqslant\left(1+\frac{\Delta t}{2}\right)\tilde{F}(n)+\Delta t\tilde{Q}(n+1). \tag{24}$$

Thus, we obtain from Eq. (24) that

$$\begin{aligned}\tilde{F}(n)&\leqslant\frac{1+\frac{\Delta t}{2}}{1-\frac{\Delta t}{2}}\tilde{F}(n-1)+\frac{\Delta t}{1-\frac{\Delta t}{2}}\tilde{Q}(n)\\&\leqslant\frac{1+\frac{\Delta t}{2}}{1-\frac{\Delta t}{2}}\left[\frac{1+\frac{\Delta t}{2}}{1-\frac{\Delta t}{2}}\tilde{F}(n-2)+\frac{\Delta t}{1-\frac{\Delta t}{2}}\tilde{Q}(n-1)\right]+\frac{\Delta t}{1-\frac{\Delta t}{2}}\tilde{Q}(n)\\&\leqslant\cdots\\&\leqslant\left(\frac{1+\frac{\Delta t}{2}}{1-\frac{\Delta t}{2}}\right)^n\tilde{F}(0)+\frac{\Delta t}{1-\frac{\Delta t}{2}}\left[1+\left(\frac{1+\frac{\Delta t}{2}}{1-\frac{\Delta t}{2}}\right)+\left(\frac{1+\frac{\Delta t}{2}}{1-\frac{\Delta t}{2}}\right)^2+\cdots+\left(\frac{1+\frac{\Delta t}{2}}{1-\frac{\Delta t}{2}}\right)^{n-1}\right]\max_{0\leqslant k\leqslant n}\tilde{Q}(k)\\&=\left(\frac{1+\frac{\Delta t}{2}}{1-\frac{\Delta t}{2}}\right)^n\tilde{F}(0)+\frac{\Delta t}{1-\frac{\Delta t}{2}}\left[\frac{1-(\frac{1+\frac{\Delta t}{2}}{1-\frac{\Delta t}{2}})^n}{1-(\frac{1+\frac{\Delta t}{2}}{1-\frac{\Delta t}{2}})}\right]\max_{0\leqslant k\leqslant n}\tilde{Q}(k)\\&=\left(\frac{1+\frac{\Delta t}{2}}{1-\frac{\Delta t}{2}}\right)^n\tilde{F}(0)-\left[1-\left(\frac{1+\frac{\Delta t}{2}}{1-\frac{\Delta t}{2}}\right)^n\right]\max_{0\leqslant k\leqslant n}\tilde{Q}(k)\\&\leqslant\left(\frac{1+\frac{\Delta t}{2}}{1-\frac{\Delta t}{2}}\right)^n\left[\tilde{F}(0)+\max_{0\leqslant k\leqslant n}\tilde{Q}(k)\right].\end{aligned} \tag{25}$$

Here, the used equal sign in the above derivation indicates to find the sum of a geometric series and to simplify the equation. Using the inequalities $(1+\varepsilon)^n\leqslant e^{n\varepsilon}$ for $\varepsilon>0$, and $(1-\varepsilon)^{-1}\leqslant e^{2\varepsilon}$ when $0<\varepsilon\leqslant\frac{1}{2}$, we obtain for sufficiently small Δt,

$$\begin{aligned}\tilde{F}(n)&\leqslant e^{n\frac{\Delta t}{2}}\cdot e^{n\Delta t}\left[\tilde{F}(0)+\max_{0\leqslant k\leqslant n}\tilde{Q}(k)\right]\\&\leqslant e^{\frac{3n\Delta t}{2}}\left[\tilde{F}(0)+\max_{0\leqslant k\leqslant n}\tilde{Q}(k)\right].\end{aligned} \tag{26}$$

Hence, the solution of the scheme, Eqs. (15)–(18), satisfies, when Δt is sufficiently small,

$$\begin{aligned}&\Delta x\sum_{i=1}^{N}C_i\sum_{m=1}^{M-1}\left[(T_i)_m^n\right]^2\\&\leqslant e^{\frac{3}{2}n\Delta t}\cdot\left\{\Delta x\sum_{i=1}^{N}C_i\sum_{m=1}^{M-1}\left[(T_i)_m^0\right]^2+\max_{0\leqslant k\leqslant n}\Delta x\sum_{i=1}^{N}\sum_{m=1}^{M-1}\frac{1}{C_i}\left[(Q_i)_m^{k+\frac{1}{2}}\right]^2\right\},\end{aligned} \tag{27}$$

for any n in $0\leqslant n\Delta t\leqslant t_0$.

Eq. (27) can be considered as a discrete analogue of Eq. (14). Using the discrete energy estimate, one may obtain that the scheme, Eqs. (15)–(18), is unconditionally stable. Indeed, if we assume that $(T_i)_m^n$ and $(\hat{T}_i)_m^n$ are the numerical solutions obtained based on the different initial conditions, $(T_i)_m^0$ and $(\hat{T}_i)_m^0$, and different heat sources, $(Q_i)_m^{n+\frac{1}{2}}$ and $(\hat{Q}_i)_m^{n+\frac{1}{2}}$, respectively, and the same boundary conditions, then letting $(E_i)_m^n=(T_i)_m^n-(\hat{T}_i)_m^n$ and $(\varepsilon_i)_m^{n+\frac{1}{2}}=(Q_i)_m^{n+\frac{1}{2}}-(\hat{Q}_i)_m^{n+\frac{1}{2}}$, one may see from Eqs. (15)–(18) that $(E_i)_m^n$ and $(\varepsilon_i)_m^{n+\frac{1}{2}}$ satisfy

$$\begin{aligned}&C_1\frac{(E_1)_m^{n+1}-(E_1)_m^n}{\Delta t}\\&=\nabla_x\cdot\left[(k_1)_{m-\frac{1}{2}}^{n+\frac{1}{2}}\nabla_{\bar{x}}\left(\frac{(E_1)_m^{n+1}+(E_1)_m^n}{2}\right)\right]\\&\quad-\sum_{i=2}^{N}G_{1,i}\left[\frac{(E_1)_m^{n+1}+(E_1)_m^n}{2}-\frac{(E_i)_m^{n+1}+(E_i)_m^n}{2}\right]\\&\quad+(\varepsilon_1)_m^{n+\frac{1}{2}},\end{aligned} \tag{28}$$

$$\begin{aligned}&C_j\frac{(E_j)_m^{n+1}-(E_j)_m^n}{\Delta t}\\&=\nabla_x\cdot\left[(k_j)_{m-\frac{1}{2}}^{n+\frac{1}{2}}\nabla_{\bar{x}}\left(\frac{(E_j)_m^{n+1}+(E_j)_m^n}{2}\right)\right]\\&\quad+\sum_{i=1}^{j-1}G_{i,j}\left[\frac{(E_i)_m^{n+1}+(E_i)_m^n}{2}-\frac{(E_j)_m^{n+1}+(E_j)_m^n}{2}\right]\\&\quad-\sum_{i=j+1}^{N}G_{j,i}\left[\frac{(E_j)_m^{n+1}+(E_j)_m^n}{2}-\frac{(E_i)_m^{n+1}+(E_i)_m^n}{2}\right]+(\varepsilon_j)_m^{n+\frac{1}{2}},\\&j=2,\ldots,N-1,\end{aligned} \tag{29}$$

$$\begin{aligned}&C_N\frac{(E_N)_m^{n+1}-(E_N)_m^n}{\Delta t}\\&=\nabla_x\cdot\left[(k_N)_{m-\frac{1}{2}}^{n+\frac{1}{2}}\nabla_{\bar{x}}\left(\frac{(E_N)_m^{n+1}+(E_N)_m^n}{2}\right)\right]\\&\quad+\sum_{i=1}^{N-1}G_{i,N}\left[\frac{(E_i)_m^{n+1}+(E_i)_m^n}{2}-\frac{(E_N)_m^{n+1}+(E_N)_m^n}{2}\right]+(\varepsilon_N)_m^{n+\frac{1}{2}}.\end{aligned} \tag{30}$$

Hence, we conclude that $(E_i)_m^n$ and $(\varepsilon_i)_m^{n+\frac{1}{2}}$ should satisfy the discrete energy estimate, Eq. (27),

$$\begin{aligned}&\Delta x\sum_{i=1}^{N}C_i\sum_{m=1}^{M-1}\left[(E_i)_m^n\right]^2\\&\leqslant e^{\frac{3}{2}t_0}\cdot\left\{\Delta x\sum_{i=1}^{N}C_i\sum_{m=1}^{M-1}\left[(E_i)_m^0\right]^2+\max_{0\leqslant k\leqslant n}\Delta x\sum_{i=1}^{N}\sum_{m=1}^{M-1}\frac{1}{C_i}\left[(\varepsilon_i)_m^{k+\frac{1}{2}}\right]^2\right\},\end{aligned} \tag{31}$$

for any n in $0\leqslant n\Delta t\leqslant t_0$. Because there is no restriction on the mesh ratio, Eq. (31) implies that the scheme is unconditionally stable with respect to the initial condition and the heat source.

It should be pointed out that the above finite difference scheme can be easily generalized to two- and three-dimensional cases.

4. Numerical examples

To test the applicability of the scheme, we first consider a simple dimensionless 1D three-carrier system as follows:

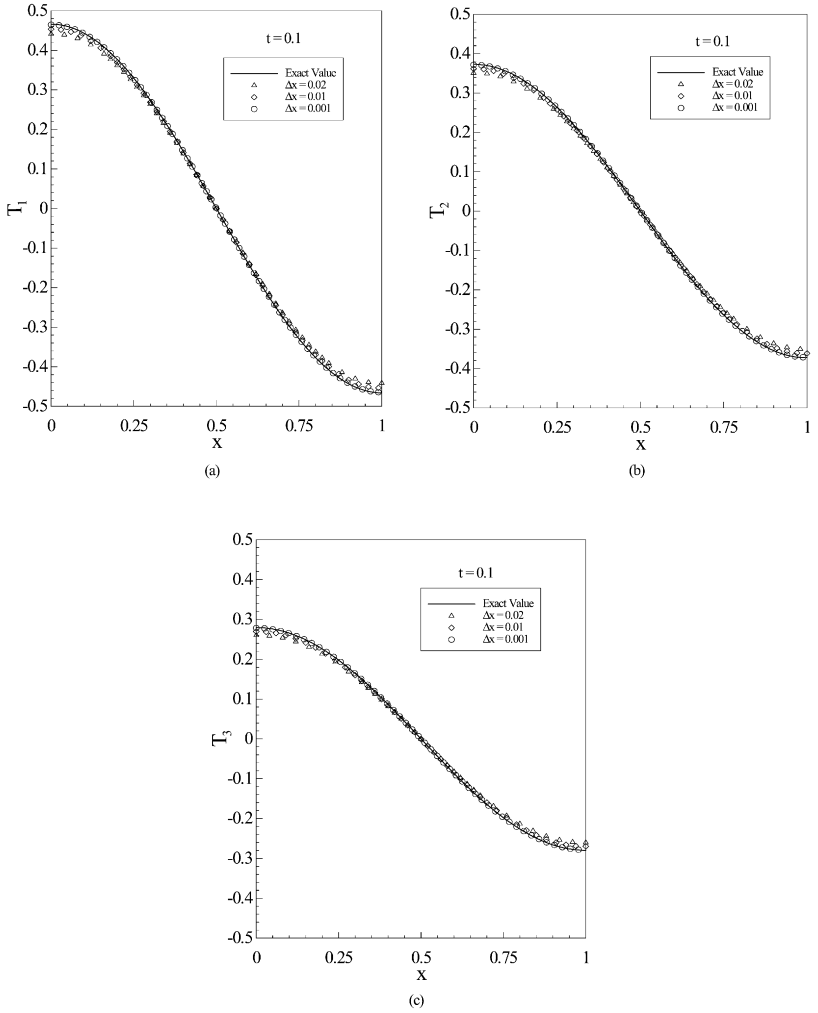

Fig. 2. Numerical solutions (a) T_1, (b) T_2, and (c) T_3, and the corresponding exact solutions at $t = 0.1$ obtained using three different grid sizes.

$$\frac{\partial T_1}{\partial t} = \frac{\partial^2 T_1}{\partial x^2} - \pi^2(T_1 - T_2) - \pi^2(T_1 - T_3) + 2\pi^2 e^{-\pi^2 t}\cos\pi x, \tag{32a}$$

$$\frac{\partial T_2}{\partial t} = 2\frac{\partial^2 T_2}{\partial x^2} + \pi^2(T_1 - T_2) - \pi^2(T_2 - T_3) + \pi^2 e^{-\pi^2 t}\cos\pi x, \tag{32b}$$

$$\frac{\partial T_3}{\partial t} = 2\frac{\partial^2 T_3}{\partial x^2} + \pi^2(T_1 - T_3) + \pi^2(T_2 - T_3), \tag{32c}$$

where $0 \leqslant x \leqslant 1$. The boundary condition is $\frac{\partial T_i(0,t)}{\partial x} = \frac{\partial T_i(1,t)}{\partial x} = 0$, $i = 1, 2, 3$. The initial conditions are $T_1 = \frac{5}{4}\cos\pi x$, $T_2 = \cos\pi x$, and $T_3 = \frac{3}{4}\cos\pi x$. It can be seen that the exact solutions of the system are $T_1 = \frac{5}{4}e^{-\pi^2 t}\cos\pi x$, $T_2 = e^{-\pi^2 t}\cos\pi x$, and $T_3 = \frac{3}{4}e^{-\pi^2 t}\cos\pi x$. Furthermore, using a simple integration, one may see that the energy estimate in Eq. (14) is held.

In our computation, we chose $\Delta t = 0.001$ and $\Delta x = 0.02, 0.01, 0.001$, respectively. To obtain the numerical solutions, we employed a Gauss–Seidel type iteration coupled with Thomas' algorithm for solving tridiagonal linear systems.

Figs. 2–4 show the numerical solutions of T_1, T_2 and T_3, and the corresponding exact solutions at $t = 0.1, 0.2, 1.0$, respectively. It can be seen from these figures that the numerical solutions are close to the exact solutions with the decrease of grid size Δx, implying that the numerical scheme is stable and accurate.

To validate the relation in Eq. (27), we computed the energy terms on both sides in Eq. (27) based on this example, as shown in Fig. 5. Result shows that the energy on the LHS is much smaller than that on the RHS in Eq. (27), implying that Eq. (27) is held.

We further consider a dimensionless 2D three-carrier system as follows:

$$\frac{\partial T_1}{\partial t} = 2\left(\frac{\partial^2 T_1}{\partial x^2} + \frac{\partial^2 T_1}{\partial y^2}\right) - \pi^2(T_1 - T_2) - \pi^2(T_1 - T_3) + 2\pi^2 e^{-\pi^2 t}\cos\pi x\cos\pi y, \tag{33a}$$

$$\frac{\partial T_2}{\partial t} = 2\left(\frac{\partial^2 T_2}{\partial x^2} + \frac{\partial^2 T_2}{\partial y^2}\right) + \pi^2(T_1 - T_2) - \pi^2(T_2 - T_3) + \pi^2 e^{-\pi^2 t}\cos\pi x\cos\pi y, \tag{33b}$$

$$\frac{\partial T_3}{\partial t} = 2\left(\frac{\partial^2 T_3}{\partial x^2} + \frac{\partial^2 T_3}{\partial y^2}\right) + \pi^2(T_1 - T_3) + \pi^2(T_2 - T_3), \tag{33c}$$

where $0 \leqslant x \leqslant 1$ and $0 \leqslant y \leqslant 1$. The boundary conditions are $\frac{\partial T_i(0,y,t)}{\partial x} = \frac{\partial T_i(1,y,t)}{\partial x} = 0$ and $\frac{\partial T_i(x,0,t)}{\partial y} = \frac{\partial T_i(x,1,t)}{\partial y} = 0$, $i = 1, 2, 3$. The exact solutions of the system are $T_1 = \frac{1}{2}e^{-\pi^2 t}\cos\pi x\cos\pi y$, $T_2 = \frac{1}{3}e^{-\pi^2 t}\cos\pi x\cos\pi y$, and $T_3 = \frac{1}{6}e^{-\pi^2 t}\cos\pi x\cos\pi y$, where the initial conditions are obtained based on the exact solutions. In our computation, we chose $\Delta t = 0.001$ and $h = \Delta x = \Delta y = 0.1, 0.05, 0.01$, respectively.

Figs. 6–8 show the numerical solutions of T_1, T_2 and T_3 along the line $x = 0$ (the solutions along the line $y = 0$ are the same

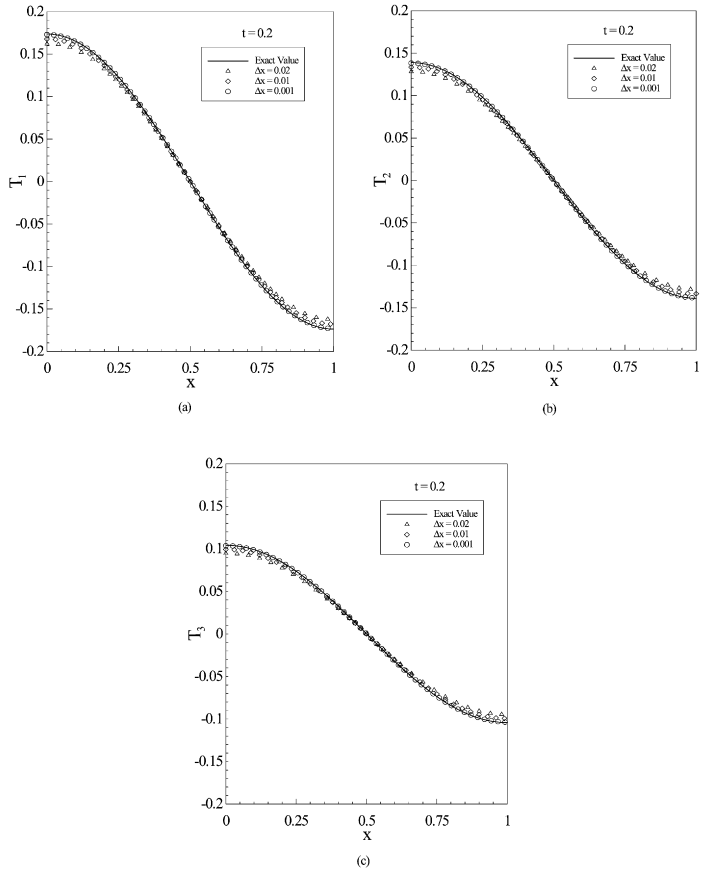

Fig. 3. Numerical solutions (a) T_1, (b) T_2, and (c) T_3, and the corresponding exact solutions at $t = 0.2$ obtained using three different grid sizes.

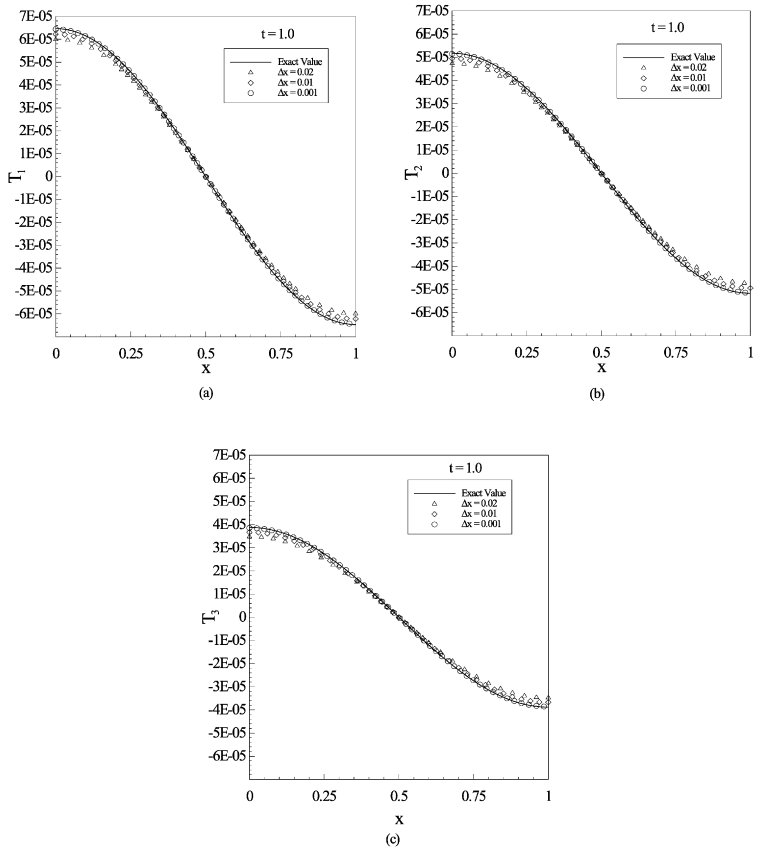

Fig. 4. Numerical solutions (a) T_1, (b) T_2, and (c) T_3, and the corresponding exact solutions at $t = 1.0$ obtained using three different grid sizes.

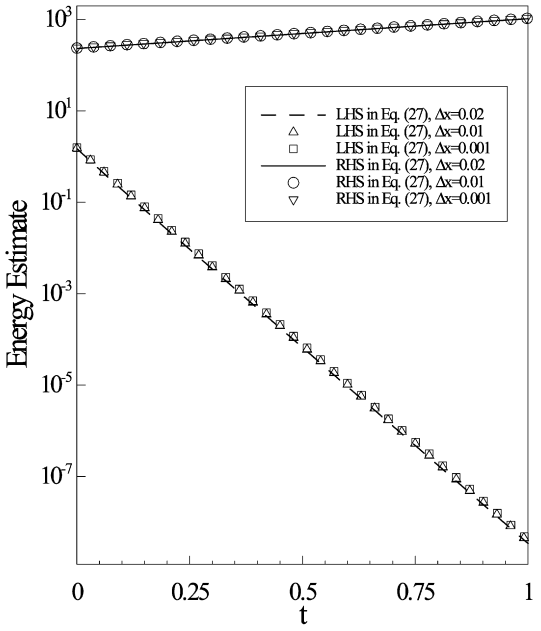

Fig. 5. Comparison of energy estimates both sides in Eq. (27).

Table 1
Errors in l_2-norm between the numerical solutions and the corresponding exact solutions.

(a) $T_1(x, y, t)$			
$h\backslash t$	0.1	0.2	1.0
0.1	2.3543e–2	8.8918e–3	3.3086e–6
0.05	1.0915e–2	4.1671e–3	1.5250e–6
0.01	2.0396e–3	7.8742e–4	2.1089e–7
(b) $T_2(x, y, t)$			
$h\backslash t$	0.1	0.2	1.0
0.1	1.7728e–2	6.7233e–3	2.5022e–6
0.05	8.4237e–3	3.2375e–3	1.1866e–6
0.01	1.6035e–3	6.2480e–4	1.8412e–7
(c) $T_c(x, y, t)$			
$h\backslash t$	0.1	0.2	1.0
0.1	1.1932e–2	4.5622e–3	1.6984e–6
0.05	5.9391e–3	2.3106e–3	8.4982e–7
0.01	1.1683e–3	4.6257e–4	1.6136e–7

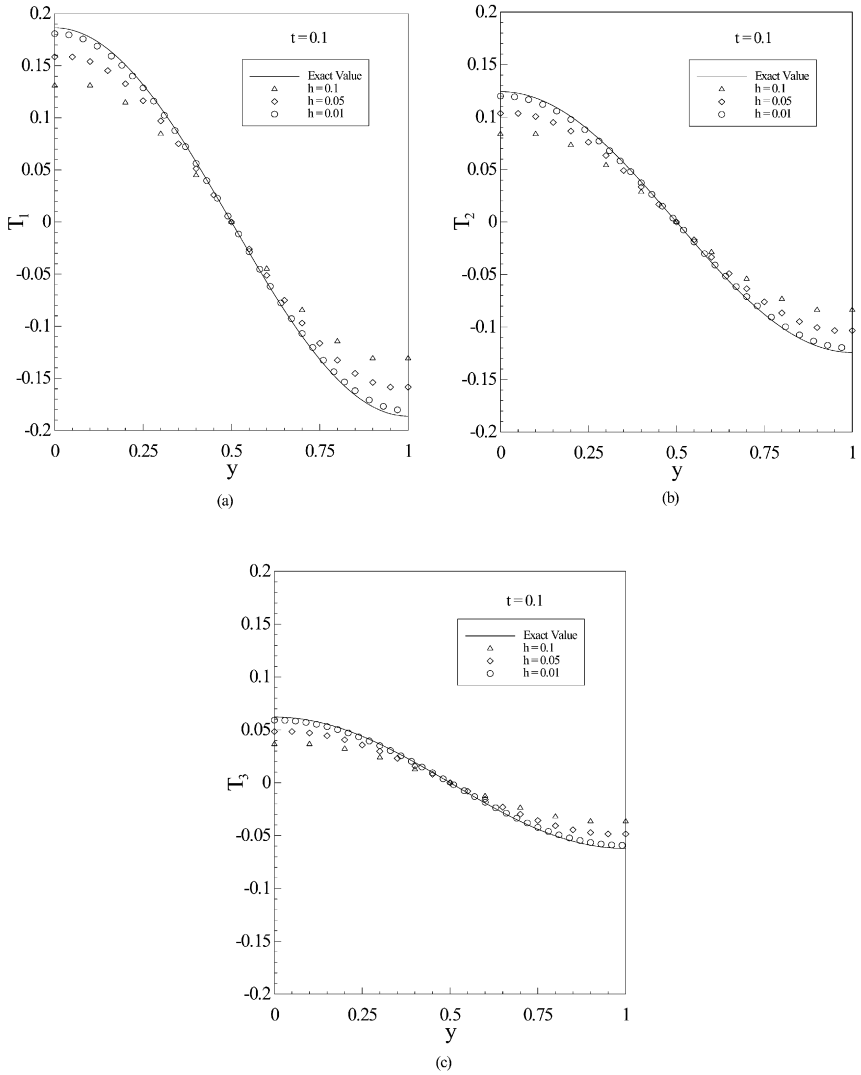

Fig. 6. Numerical solutions (a) T_1, (b) T_2, and (c) T_3, and the corresponding exact solutions along the line $x = 0$ at $t = 0.1$ obtained using three different grid sizes.

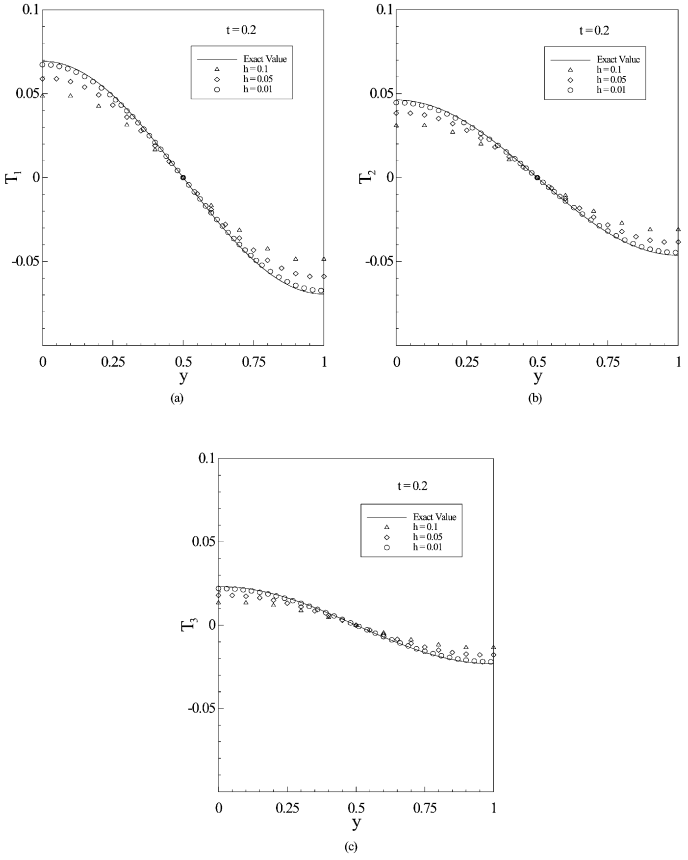

Fig. 7. Numerical solutions (a) T_1, (b) T_2, and (c) T_3, and the corresponding exact solutions along the line $x = 0$ at $t = 0.2$ obtained using three different grid sizes.

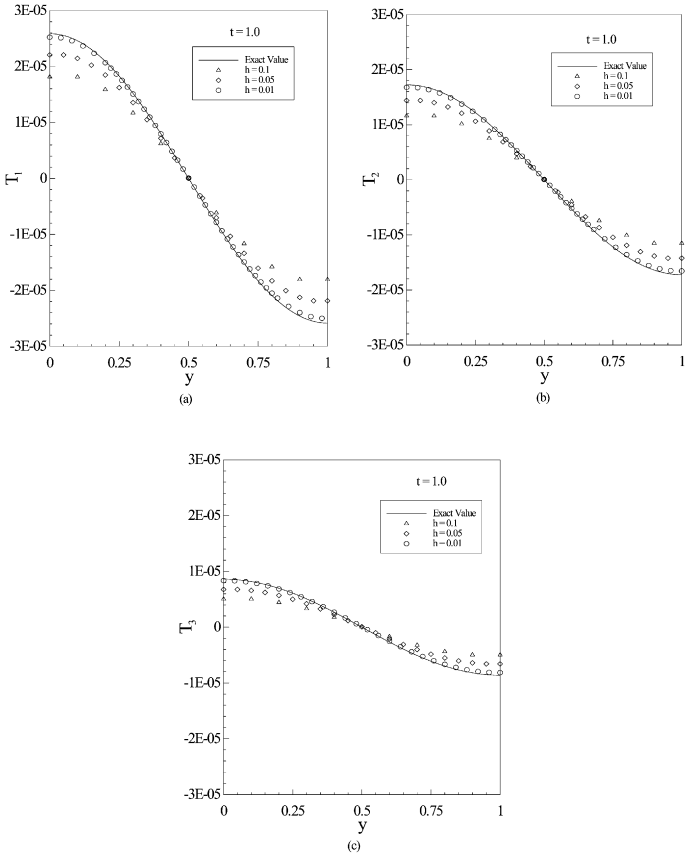

Fig. 8. Numerical solutions (a) T_1, (b) T_2, and (c) T_3, and the corresponding exact solutions along the line $x = 0$ at $t = 1.0$ obtained using three different grid sizes.

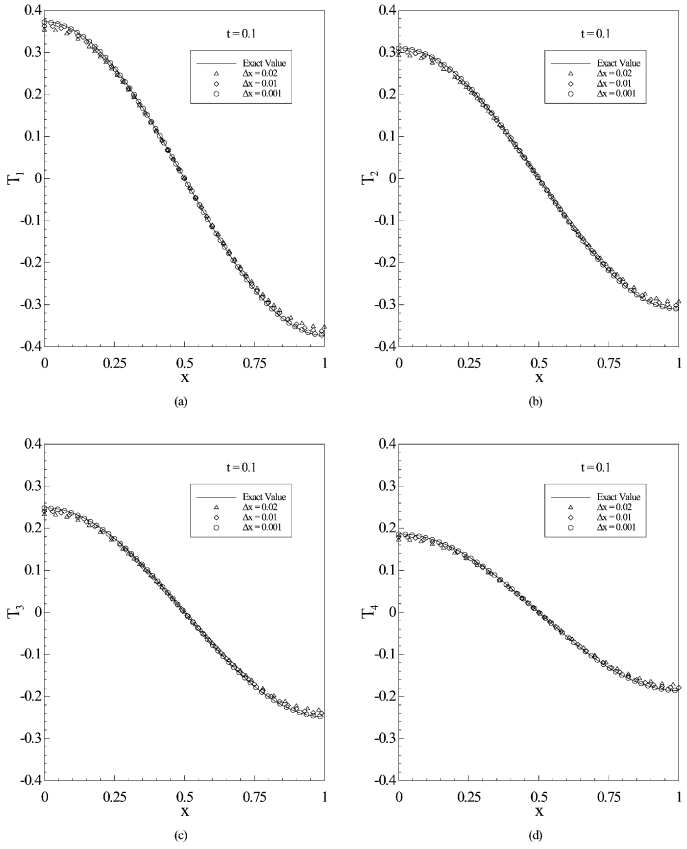

Fig. 9. Numerical solutions (a) T_1, (b) T_2, (c) T_3, and (d) T_4, and the corresponding exact solutions at $t = 0.1$ obtained using three different grid sizes.

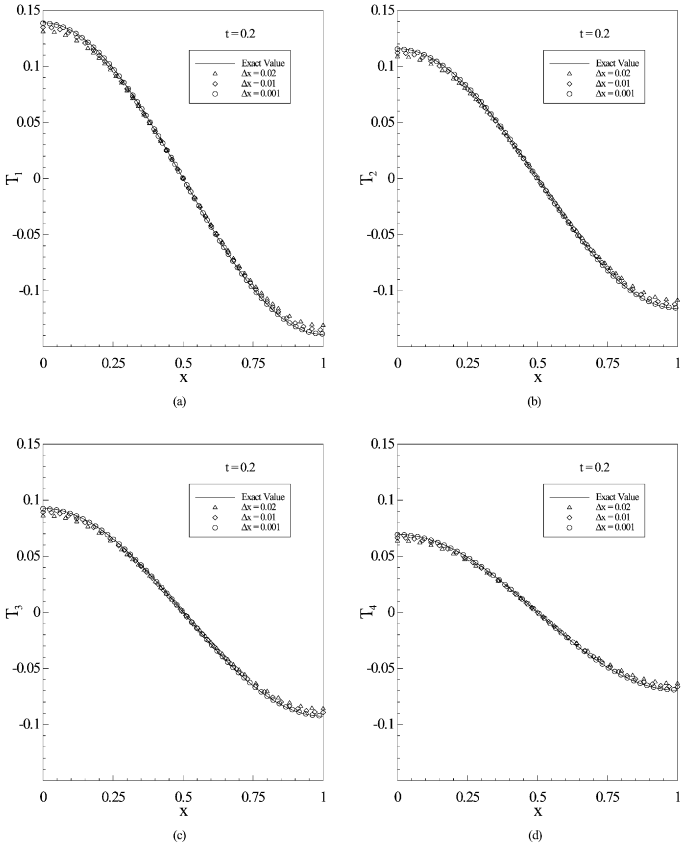

Fig. 10. Numerical solutions (a) T_1, (b) T_2, (c) T_3,and (d) T_4, and the corresponding exact solutions at $t = 0.2$ obtained using three different grid sizes.

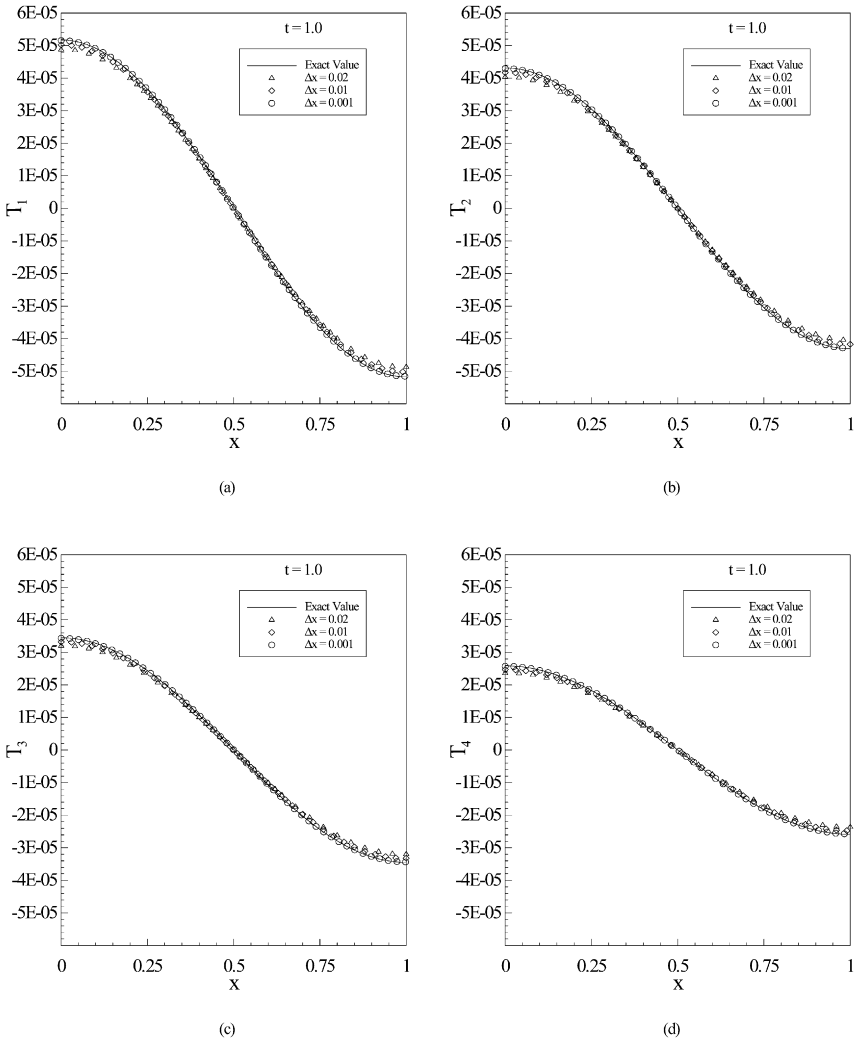

Fig. 11. Numerical solutions (a) T_1, (b) T_2, (c) T_3, and (d) T_4, and the corresponding exact solutions at $t = 1.0$ obtained using three different grid sizes.

because of symmetry), and the corresponding exact solutions at $t = 0.1, 0.2, 1.0$, respectively. Table 1 lists the errors in l_2-norm ($i.e.$, error $= \{h^2 \sum_{j,k}[(T_i^{\text{numerical}})_{jk} - (T_i^{\text{exact}})_{jk}]^2\}^{\frac{1}{2}}$, $i = 1, 2, 3$) between the numerical solutions and the corresponding exact solutions of T_1, T_2 and T_3, respectively. Again, it can be seen from these figures and the table that the numerical solutions are close to the exact solutions with the decrease of grid size h, implying that the numerical scheme is stable and accurate.

Finally, we consider a dimensionless 1D four-carrier system as follows:

$$\frac{\partial T_1}{\partial t} = 3\frac{\partial^2 T_1}{\partial x^2} - \pi^2(T_1 - T_2) - \pi^2(T_1 - T_3) - \pi^2(T_1 - T_4) + 3\pi^2 e^{-\pi^2 t}\cos\pi x, \quad (34a)$$

$$\frac{\partial T_2}{\partial t} = 3\frac{\partial^2 T_2}{\partial x^2} + \pi^2(T_1 - T_2) - \pi^2(T_2 - T_3) - \pi^2(T_2 - T_4) + 2\pi^2 e^{-\pi^2 t}\cos\pi x, \quad (34b)$$

$$\frac{\partial T_3}{\partial t} = 3\frac{\partial^2 T_3}{\partial x^2} + \pi^2(T_1 - T_3) + \pi^2(T_2 - T_3) - \pi^2(T_3 - T_4) + \pi^2 e^{-\pi^2 t}\cos\pi x, \quad (34c)$$

$$\frac{\partial T_4}{\partial t} = 3\frac{\partial^2 T_4}{\partial x^2} + \pi^2(T_1 - T_4) + \pi^2(T_2 - T_4) + \pi^2(T_3 - T_4), \quad (34d)$$

where $0 \leqslant x \leqslant 1$. The boundary condition is $\frac{\partial T_i(0,t)}{\partial x} = \frac{\partial T_i(1,t)}{\partial x} = 0$, $i = 1, 2, 3, 4$. The exact solutions of the system are $T_1 = e^{-\pi^2 t}\cos\pi x$, $T_2 = \frac{5}{6}e^{-\pi^2 t}\cos\pi x$, $T_3 = \frac{2}{3}e^{-\pi^2 t}\cos\pi x$ and $T_4 = \frac{1}{2}e^{-\pi^2 t}\cos\pi x$, where the initial conditions are obtained based on the exact solutions. In our computation, we chose $\Delta t = 0.001$ and $\Delta x = 0.02, 0.01, 0.001$, respectively.

Figs. 9–11 show the numerical solutions of T_1, T_2, T_3 and T_4, and the corresponding exact solutions at $t = 0.1, 0.2, 1.0$, respectively. Again, it can be seen from these figures that the numerical solutions are close to the exact solutions with the decrease of grid size Δx, implying that the numerical scheme is stable and accurate.

It will be interesting to apply our N-carrier system to a realistic engineering application. Unfortunately, we have not found such an example since the values of coupling factors $\{G_{i,j}\}$ have not yet been determined in realistic engineering applications and the ongoing research is still at an early stage.

5. Conclusion

We have proposed a generalized N-carrier system which is shown to satisfy an energy estimate. Based on the energy estimate, a finite difference scheme for thermal analysis in the multi-carrier system has been developed. The scheme has been proven to satisfy a discrete analogue of the energy estimate, implying that it is

unconditionally stable. Numerical results coincide with the theoretical analysis.

References

[1] M.I. Kaganov, I.M. Lifshitz, M.V. Tanatarov, Relaxation between electrons and crystalline lattices, Sov. Phys. JETP 4 (1957) 173–187.

[2] S.I. Anisimov, B.L. Kapeliovich, T.L. Perel'man, Electron emission from metal surfaces exposed to ultra-short laser pulses, Sov. Phys. JETP 39 (1974) 375–377.

[3] T.Q. Qiu, C.L. Tien, Short-pulse laser heating on metals, Int. J. Heat Mass Transfer 35 (1992) 719–726.

[4] T.Q. Qiu, C.L. Tien, Heat transfer mechanisms during short-pulse laser heating of metals, ASME J. Heat Mass Transfer 115 (1993) 835–841.

[5] D.Y. Tzou, A unified field approach for heat conduction from micro to macroscales, ASME J. Heat Mass Transfer 117 (1995) 8–16.

[6] D.Y. Tzou, Macro- to Microscale Heat Transfer: The Lagging Behavior, Taylor & Francis, Washington DC, 1997 (Ch. 2).

[7] J.K. Chen, J.E. Beraum, Numerical study of ultrashort laser pulse interactions with metal films, Numer. Heat Transfer A 40 (2001) 1–20.

[8] W.J. Minkowycz, A. Haji-Sheikhb, K. Vafai, On departure from local thermal equilibrium in porous media due to a rapidly changing heating source: the Sparrow number, Int. J. Heat Mass Transfer 42 (1999) 3373–3385.

[9] D.Y. Tzou, J.K. Chen, Thermal lagging in random media, AIAA J. Thermophys. Heat Transfer 12 (1998) 567–574.

[10] A. Faghri, Y. Zhang, Transport Phenomena in Multiphase Systems, Elsevier, UK, 2006.

[11] F. Dausinger, F. Lichtner, H. Lubatschowdki, Femtosecond Technology for Technical and Medical Applications, Springer-Verlag, Berlin, Germany, 2004.

[12] D.Y. Tzou, Thermal lagging: multi-component systems and thermoelectric coupling, in: Proceedings of the First ASME Micro/Nanoscale Heat Transfer International Conference (MNHT08), Tainan, Taiwan, January 6–9, 2008.

[13] L.C. Evans, Partial Differential Equations, American Mathematical Society, Providence, Rhode Island, 1998, pp. 624–628.

[14] K.E. Atkinson, W. Han, Theoretical Numerical Analysis: A Function Analysis Framework, 2nd ed., Texts in Applied Mathematics, vol. 39, Springer, 2005.

[15] J. Strikwerda, Finite Difference Schemes and Partial Differential Equations, 2nd ed., SIAM, Philadelphia, 2004.

[16] J.W. Thomas, Numerical Partial Differential Equations: Finite Difference Methods, Texts in Applied Mathematics, vol. 22, Springer, 2004.